Hindawi
International Journal of Photoenergy
Volume 2023, Article ID 4717110, 17 pages
https://doi.org/10.1155/2023/4717110

Research Article

Application of Deep Learning to the Prediction of Solar Irradiance through Missing Data

R. Girimurugan,[1] P. Selvaraju,[2] Prabahar Jeevanandam,[3] M. Vadivukarassi,[4] S. Subhashini,[5] N. Selvam,[6] S. K. Hasane Ahammad,[7] S. Mayakannan,[8] and Selvakumar Kuppusamy Vaithilingam[9]

[1]*Department of Mechanical Engineering, Nandha College of Technology, Perundurai, Erode, Tamil Nadu, India*
[2]*Department of Mathematics, Rajalakshmi Institute of Technology, Chennai, Tamil Nadu, India*
[3]*Department of Mechanical Engineering, Park College of Engineering and Technology, Kaniyur, Coimbatore 641659, India*
[4]*Department of Computer Science Engineering, St. Martin's Engineering College, Secunderabad, Telangana, India*
[5]*Department of Computer Science and Engineering, B S Abdur Rahman Crescent Institute of Science and Technology, Vandalur, Chennai, Tamil Nadu, India*
[6]*Department of Electrical and Electronics Engineering, M.Kumarasamy College of Engineering, Karur, Tamil Nadu, India*
[7]*Department of Electronics and Communication Engineering, Koneru Lakshmaiah Education Foundation, Guntur, Andhra Pradesh, India*
[8]*Department of Mechanical Engineering, Vidyaa Vikas College of Engineering and Technology, Tiruchengode, Namakkal, Tamil Nadu, India*
[9]*School of Chemical and Bioengineering, Dire Dawa University Institute of Technology, Dire Dawa University, Dire Dawa, Ethiopia*

Correspondence should be addressed to Selvakumar Kuppusamy Vaithilingam; selvakumar.kuppusamy@ddu.edu.et

Received 13 October 2022; Revised 19 June 2023; Accepted 30 August 2023; Published 22 September 2023

Academic Editor: Qiliang Wang

The task of predicting solar irradiance is critical in the development of renewable energy sources. This research is aimed at predicting the photovoltaic plant's irradiance or power and serving as a standard for grid stability. In practical situations, missing data can drastically diminish prediction precision. Meanwhile, it is tough to pick an appropriate imputation approach before modeling because of not knowing the distribution of datasets. Furthermore, not all datasets benefit equally from using the same imputation technique. This research suggests utilizing a recurrent neural network (RNN) equipped with an adaptive neural imputation module (ANIM) to estimate direct solar irradiance when some data is missing. Without imputed information, the typical projects' imminent 4-hour irradiance depends on gaps in antique climatic and irradiation records. The projected model is evaluated on the widely available information by simulating missing data in each input series. The performance model is assessed alternative imputation techniques under a range of missing rates and input parameters. The outcomes prove that the suggested methods perform better than competing strategies when measured by various criteria. Moreover, combine the methodology with the attentive mechanism and invent that it excels in low-light conditions.

1. Introduction

Using solar photovoltaic (PV) electricity instead of fossil fuels is an excellent way to reduce civilization's impact on the environment. Solar photovoltaic (PV) power plants use PV modules and inverters to generate electricity from the sunshine. PV modules, also known as solar panels, are made up of photovoltaic cells that convert sunlight into electricity through the photovoltaic effect. These modules are typically made up of multiple cells that are connected together and mounted onto a support structure to form an array. By 2050, experts anticipate doubling the world's installed PV

capacity [1]. Due to the inherent unpredictability of PV systems, their rapid evolution makes it difficult for us to use them effectively. Predicting irradiance with great precision helps reduce the wasteful use of resources and unnecessary expenditures. Significant progress has been made since then in the field of solar irradiance prediction [2–4]. The output of PV plants can be predicted with high accuracy by focusing on two variables: global horizontal irradiance (GHI) and direct normal irradiance (DNI). Finally, GHI can be calculated using the natural, normal incidence, and solar angles [5].

The three main methods for predicting irradiance are those based on physical mechanisms, classical statistical models, and machine learning. One such physical model is numerical weather prediction (NWP) [6]. In NWP, researchers use complex differential equations to simulate the atmosphere behavior [7]. The findings of such approaches are valid on a regional scale but do not apply to local predictions. Time series data from sources like power plants and weather satellites are crunched by data-driven methods like statistical modeling and machine learning to identify features [8, 9].

One of the most popular statistical models is the autoregressive integrated moving average model (ARIMA), which uses data order determination and optimization techniques to learn the model's parameters. Approaches like this make good use of past data and are far simpler to train than conventional physical models [10]. Priority model templates, such as the linear assumption, introduce bias into learned models that cause them to distort reality. In recent years, there has been a significant uptick in using machine learning (ML) techniques and intense learning in the renewable energy sector. Recurrent neural networks (RNNs) have effectively tackled sequence prediction challenges. Neural networks can theoretically provide approximations for any nonlinear function. Thus, model bias is reduced, and fewer assumptions about the starting model are needed compared to the prior two approaches. However, long historical connections might arise from numerical issues like vanishing gradients [11]. Gate recurrent units (GRUs) and long-short-term memories (LSTMs) are frequently utilized in RNNs to get around this problem. Enhancing the outdated recurrent neural network with forgetting update and output gates makes it possible for the network to capture a wider variety of contexts more accurately. These strategies can reduce the effects of the vanishing gradient problem by extracting more meaningful information from the sequence [12].

All of the following techniques necessitate a substantial quantity of raw data. At PV stations, irradiance data and meteorological parameters can be gathered in two common approaches [13]. Some of the most common methods are ground-based weather stations, satellite-based remote sensing, sky imagers, pyranometers and pyrheliometers, and numerical weather prediction models.

The satellite can first offer approximations of surface irradiation. The data is more comprehensive but too dispersed to be helpful. Therefore, the actual irradiance at a given location can vary. The ground station radiometer can deliver the observed data under various conditions [14]. However, there are significant gaps due to communication and instrumentation breakdowns. Similar openings can be found in the weather records. Around 50% of solar energy is lost in actual circumstances [15].

Research into imputation models used during the preprocessing of data to fill in missing information has been extensively pursued to make algorithms more useful in practice [16]. Random sampling, Kalman filters, weighted moving average (MA), persistence, and interpolation are only some of the 36 imputation methods covered, along with their impacts at various temporal frequencies and their implications for midterm horizontal solar irradiance estimates. Recently, generative adversarial networks (GAN) have been used in unsupervised imputation algorithms for photovoltaic (PV) data [17]. These methods can generate the imputed sequence during the inference phase because they employ generative models to understand the possible distribution of the data.

However, some problems with GAV approaches are challenging to fix. However, PV data is notoriously unreliable and is intricately connected to the weather. Therefore, conventional statistical methods typically only address intermittent missing values and frequently disregard the actual distribution of the data [18]. Moreover, traditional imputation techniques often impute missing values using straightforward changes of the nearest neighbor or history sequence. They will struggle more when the target changes because of the difficulty in accurately representing nonlinear, multidimensional data. However, quick action is essential for short-term irradiance forecasts. Forecasting using an unsupervised technique involves an additional, time-consuming imputation step [19]. Many parameters require specific optimization because of the unpredictable nature of the training process of a generative model, which necessitates a great deal of time and human effort. Overfitting can occur if training data imputation is performed with too much precision, reducing the practical utility of the application.

To include more data and capture any oscillations in the initial difficulty stated above, more dimensional factors and nonlinear norms are frequently employed [20–22]. The second problem necessitates a plan that simplifies the network and the process. To tackle these issues, the researcher suggests an imputed GRU (IGRU), a bidirectional gate recurrent unit that employs an adaptive neural imputation module for DNI prediction. Preimputation network and GRU were combined into a single-stage network [23]. When there are gaps in data, the preimputation network uses positional prior and delay techniques to fill them in. Subsequently, the completed series is directly encoded instead of the raw data to generate summary characteristics. This process culminates in decoding the created features to recover the desired series. During the training procedure, prediction loss is used to fine-tune the GRU and imputation module weights jointly [24, 25]. As a result, the imputation values are based on operational procedures. This is the primary distinction from approaches that fill raw data's gaps before modeling. The researcher also added a novel attention module to IGRU called attention imputed gate recurrent units (AIGRU) to help with the high-frequency volatility of irradiance data. The model now pays more attention to higher-energy information than higher-frequency information.

The following are the most significant contributions of the research:

(i) To avoid time-consuming and inefficient imputation of raw data that may be missing, the researcher suggests a method for forecasting solar irradiance straight from the missing data, which performs well under a wide range of cutting rates. The benefits of preimputation include simplifying the two-stage process into a single step, lowering the model's complexity, and achieving accuracy on par with that of alternative approaches. The two-stage process is simplified into a single step, the model's complexity is lowered, and the resulting accuracy is on par with that of alternative approaches. Second, the network parameters are learned by evaluating the accuracy with which they anticipate future events. In this way, the bias and overfitting phenomena are mitigated by preventing the mistake of an outcome acquired by the imputation technique in preprocessing from being transferred to the learners. The network parameters are learned by evaluating the accuracy with which they anticipate future events, thereby preventing the mistake of an outcome acquired by the imputation technique in preprocessing from being transferred to the learners. Finally, not many hyperparameters are needed to be modified in this method compared to others. KNN's nearest neighbors, Kalman filtering's order, and so on have a significant role in determining performance. Third, more information is required for model-based imputation than for prediction. It is challenging to have amassed enough original data in some industrial contexts to provide high-precision imputation. That is why it is possible to get meaningful findings by imputing during predicting with fewer data than with model-based imputation methods based on a priori assumptions

(ii) Researchers present a neural imputation module that is adaptable and able to produce imputation data from prediction errors. Using this module, the researcher can skip the step of calculating imputation values before making a forecast

(iii) Researchers present a missing data prediction method based on attention, which is more effective under bright light. In irradiance prediction, it aims to address the issue of uneven sample sizes between high and low radiation levels without resampling. An ensemble setting can compensate for the other models

2. Related Works

2.1. Solar Irradiance Forecast/Regression with Missing Value. In the last few years, there has been a lot of focus on missing data radiation and prediction. Since irradiance imputation has many features with more common time series imputation problems, many tried-and-true traditional approaches can be applied with slight modification. While conventional methods relied on the moment and neighborhood information, they often avoided handling missing values. To fill in the gap, the author [26] employs two techniques. For missing time series data, the author [27] uses k-nearest neighbors (KNN). When it comes to characterizing multidimensional inputs; however, these methods fall short, as they do not consider the things like the correlation between irradiance and climatic data.

Several imputations by chained equivalences and regression-built imputation approach, such as multiple linear regression representations and converse distance weightage, are compared and contrasted in the article [28]. Matrix completion is used by the author of [29] to fill in data gaps before making solar radiation predictions for the near future. Several imputation approaches are investigated by the author [30], who concludes that KNN is the best option for day-ahead forecasting of photovoltaic generation. Several publications have appeared recently that attempt to summarize and compare the effectiveness of various imputation approaches. Numerous interpolations and prediction approaches are combined, and their effects are compared by authors [31, 32]. They put each method through its paces under varying time frames for predicting and conclude that Kalman filtering (KF) is the most effective for hourly data. Recent years have seen a rise in interest in using deep learning for imputation and prediction. Generative adversarial network (GAN) is the first unsupervised deep learning model to be employed as an imputation approach in solar irradiance prediction. As with conventional methods, these take two steps—first interpolating, then using the resulting data for prediction to arrive.

2.2. Time Series Imputation. Numerous disciplines, including medicine and traffic, face the age-old challenge of filling in gaps in temporal data. Mean imputation is one type of interpolation still extensively employed because of its simplicity and effectiveness. The primary source of negative consequences brought on by the absence of imputations is the split in the frequency domain [33]. In addition, model noise in the temporal field must be tolerated well. Variational autoencoders and generative adversarial networks are two unsupervised deep-learning methods that apply generative models to uncover the underlying pattern in sequence data. Together, they apply generative models to uncover the underlying pattern in sequence data. The difference between variational autoencoders and generative adversarial networks is that GAN does not aim to maximize the hidden representation in any particular way. Another RNN-based algorithm is the self-learning approach, such as Bayesian regression and inference for time series (BRITS), where the positional information of the missing data is used to dampen the hidden layer information [20].

3. Methodology

3.1. Problem Setting. For a given multivariant time series $X = (x_1, x_n, y_n)$, the research investigates the problem of irradiance Y prediction. Multihorizon forecasting refers to the prediction of multiple future steps in the time series, specifically predicting the next m steps based on the first k steps. The goal is to construct a direct method multihorizon forecasting

model that makes comprehensive, rather than incremental, predictions of all outputs [34, 35]. Researchers have one-time series represented by x_1 and the number of feature dimensions indicated by n. The researcher zeroed down on the challenge of predicting the next m steps based on t.

The first$k$steps, where the input includes previous values for the output, researchers attribute missing data to either a communication breakdown or a malfunctioning sensor. The researcher next proceeds to define several key terms. The letter M represents the positive data for missing values, where 0 indicates no data is missing and one suggests all information is present. Additionally, M states that the missing value's time step from the nearest valid observation is denoted by δt.

3.2. Traditional Imputation Methods. Here are some of the most typical approaches taken to fill in the gap during PV prediction and the methodologies utilized for comparison during the experiments.

3.2.1. Interpolation. Averages are often interpolated by using the k values closest to the gap, and standard deviations are also estimated in this module. This method of interpolation assumes that missing values are typically located near the mean distribution or median if they were lost due to random chance. The original allocation of the variables has been warped.

3.2.2. I Matrix Factorization. A matrix X with a missing value can be broken down into two or three smaller matrices using MF. The original matrix $X\hat{}$ can then be approximated by multiplying the decomposed matrices. To complete the unique matrix $X\hat{}$, the researcher employs the values found in this estimate composites, X. To maximize the loss function J in equation, the decomposition often uses an arithmetical class technique of gradient descent.

$$J = \left\|X - X\hat{}\right\|^2 = X - \mathrm{UV}^{\top 2} = \sum_{i,j,x_i \neq \mathrm{man}} \left(x_{ij} - \sum_{l=1}^{k} u_{il} v_{jl}\right)^2. \tag{1}$$

Regularization methods, as shown in equation (2), can improve estimation accuracy.

$$\begin{aligned} J &= \left\|X - X\hat{}\right\|^2 + \frac{\beta}{2}\left(\|U\|^2 + \|V\|^2\right) \\ &= \sum_{i,j,x_i \neq \neq \mathrm{an}} \left(x_{ij} - \sum_{l=1}^{k} u_{il} v_{jl}\right)^2 + \frac{\beta}{2}\left(\sum_{i,l} u_{il}^2 + \sum_{j,l} v_{jl}^2\right). \end{aligned} \tag{2}$$

3.2.3. K-Nearest Neighbors. The distance between the samples is considered by the nearest neighbor filling concept. When there is a gap in the data, it is filled in by averaging or weighting the nearby observations. KNN is preferable to mean imputation because it is less sensitive to outliers and works better with high-dimensional data. On the downside, it is computationally and spatially intensive and cannot account for sample imbalance. KNN may be computed using

$$\tilde{x}_m = \frac{\sum_i w_l c_l}{\sum_i w_i}, \tag{3}$$

where

$$w_i = \frac{1}{d_i}. \tag{4}$$

Here, $\tilde{x}_m$ indicates the missing data. i indicates the i^{th} of designated k nearest data. d indicates the distance between two specimens.

3.2.4. Multiple Imputation by Chained Equations (MICE). Assume there are n such variables as $(x_1, x_2, ..x_n)$. The variables x_2 through x_k will be used to perform a regression on the missing x_1. In this case, the regressed values are substituted for x_1 in the expression. If x_2 is missing data, the regression model will still use x_1, x_3, and up to x_n as inputs. Later, regression estimates will be substituted for the missing values.

3.2.5. Kalman Filtering. The state space model upon which the Kalman filter is based consists of two equations [36].

$$\begin{aligned} y_t &= H_t \alpha_t + \omega_t, \\ \alpha_{t+1} &= F_t \alpha_t + \varepsilon_t, \end{aligned} \tag{5}$$

where α is for the hidden condition, y stands for the observing data, H stands for the measuring matrix, F stands for the transitional matrix, and ω and ε stand for the noise. Standard practice for interpolation involves two stages. In the first stage, the states and covariances in equation (5) are erudite depending on the observable data. In the second stage, the researcher uses the past data to make an educated guess or smooth the future goal. For this purpose, the researcher employs Kalman filtering's smoothing technique.

3.3. IGRU and AIGRU. Two different approaches are presented here. For starters, the researcher presents the neural imputation module, any predictive model with imputation capabilities. Then, a neural imputation module for GRU and the rationale for employing a bidirectional structure are shown. The paper concludes by introducing an attention-based GRU with a neural imputation module.

3.3.1. Module for Neural Imputation. To better handle missing data, researchers in the current paper develop an adaptive imputation unit in a neural network. When dealing with missing data, researchers presume that the location of the missing data is either known empirically or using techniques like irregularity finding or that the position range is nil. In post-apocalyptic scenarios, for instance, the radiometer readings may show up as long stretches of zeros between sunrise and sunset. For example, suppose raw data are fed into a neural network without preprocessing. In that case,

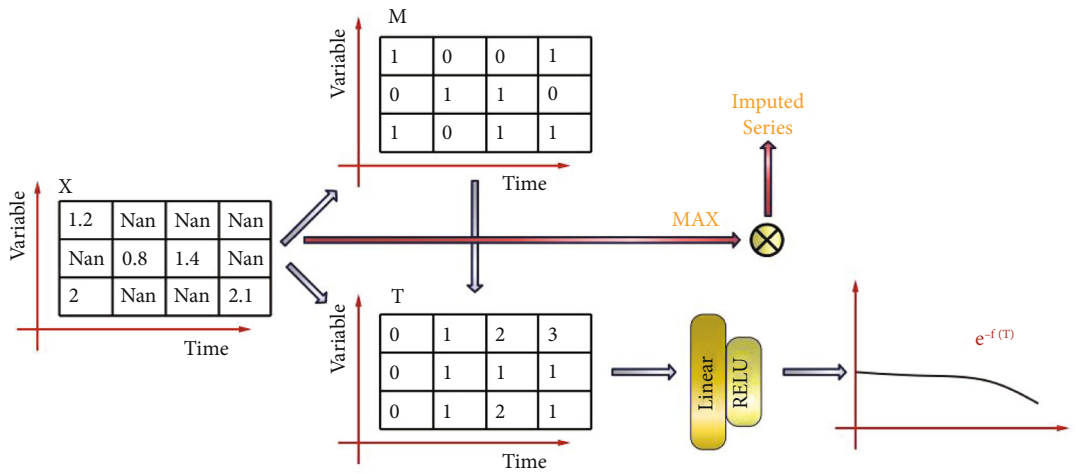

Figure 1: The imputation flow.

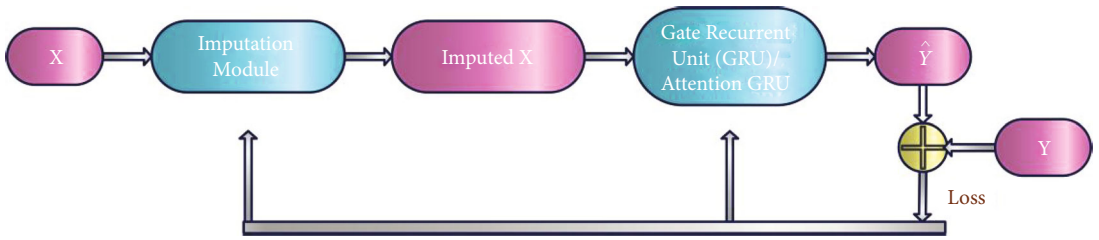

Figure 2: The path of loss.

the model may incorrectly infer features based on a high proportion of missing values in the input and the supervised data.

The law of large numbers states that gaps in data are typically filled in by values close to the most recent measurements. The missing step δ in equation (6) defines the decay coefficient as γ.

$$\gamma_t = \mathbf{exp}\left\{-\mathrm{m}\left(\mathbf{0}, \mathbf{W}_\gamma \boldsymbol{\delta}_t + \mathbf{b}_\gamma\right)\right\}, \tag{6}$$

where the linear coefficient and bias for the missing stage δ are denoted by $\mathbf{W}_\gamma$ and $\mathbf{b}_\gamma$. In the first place, the step size is linearly transformed. Afterward, the activation function places constraints on the altered result, checking that γ is not equivalent to one and is not equal to nil. The process on the right-hand side of this equation does not have to be exponential; rather, it can be any member of a class of monotonically decreasing functions. If the decline is monotonic, then the more significant the δ missing values relative to the last observation, the lesser the γ, and the higher the decay.

$$\mathbf{x}_t = \mathrm{m}_t \odot \mathbf{x}_t + (1 - \mathrm{m}_t) \odot (\gamma_t \bar{x}_t). \tag{7}$$

The estimated, $\mathbf{x}_t$ incorporates both the actual value and the imputed values after missing information has been "filled in." The researcher may generate a new estimate if the researcher knows the time step of the preceding observation and the largest possible range within the observation window. The nearest observation is insufficient since it is not easy to guarantee that the missing value is less than the most relative value. That is why it makes sense to use historical data, like the highest value during the preceding days, by considering the maximum observation inside the period. Looking at Figure 1 shows a simplified version of the imputation procedure.

The revised estimates are fed into the model. All the network weightage, such as the linear factors in the decay coefficients and the missing step coefficients, is learned by backpropagation during the training process. A reliable estimate for the missing data will result from this. The overall algorithm flow and the loss propagation track are displayed in Figure 2.

3.3.2. IGRU. An in-depth description of GRU is provided here. GRU is a type of recurrent neural network, a kind of neural network structure typically employed in sequence modeling. To solve sequence problems, RNNs rely on a crucial component: memory state neurons. These neurons' job is to memorize past events, and the researcher may express them as generalities using equation (8).

$$b_t = f(b_{t-1}, y_t, x_t), \tag{8}$$

where b is the hidden-layer neuron's value and f is the update function that must be memorized.

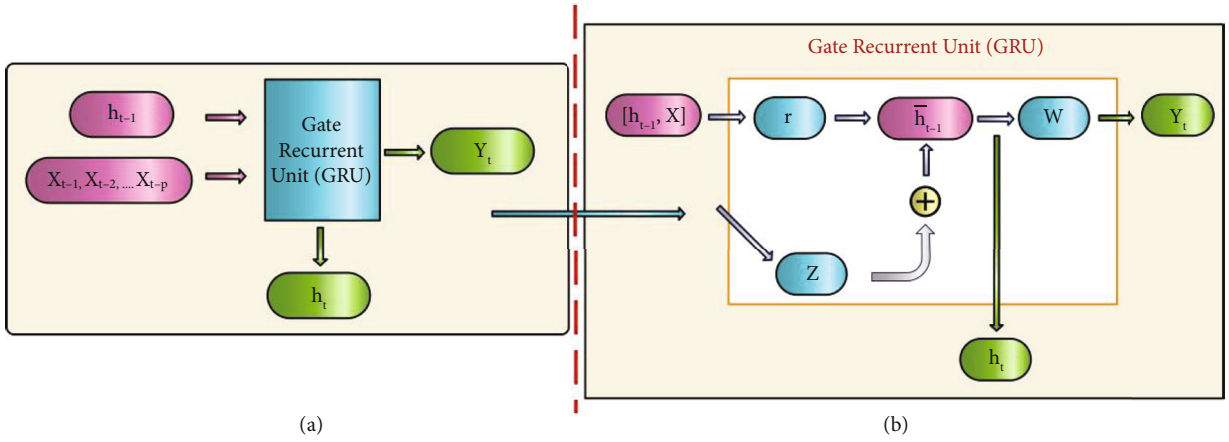

Figure 3: GRU's structural arrangement. (a) The GRU's input and output and (b) the GRU cell's internal structure.

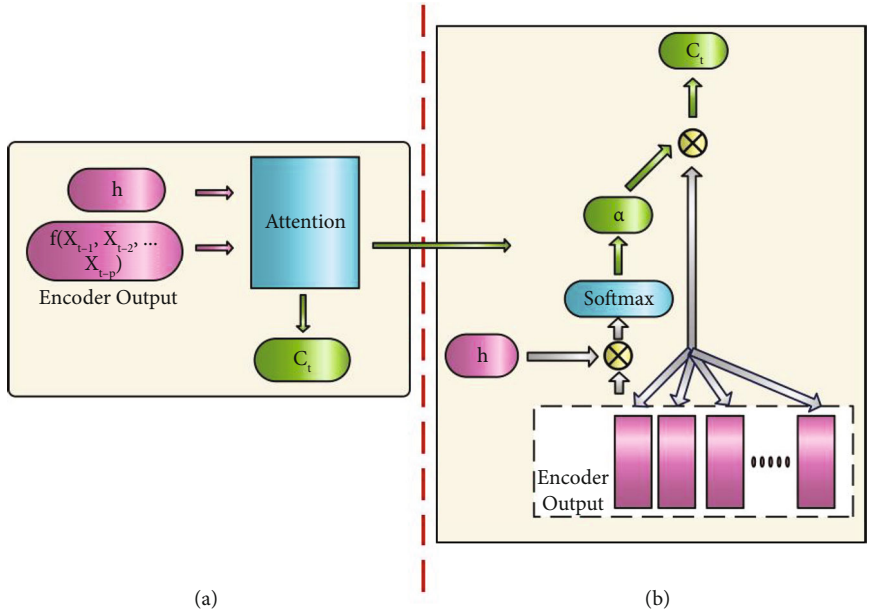

Figure 4: Mechanism for attention. (a) Input(I\P) and output(O/P) of the attention unit and (b) internal structure of the attention unit.

Both an update gate and a reset gate are labeled f in the GRU model. Equated to LSTM, the memory is guaranteed, and gradient disappearance is reduced with fewer parameters and faster training.

$$r_t = \sigma(W_r \cdot [b_{t-1}, x_t]), \tag{9}$$

$$z_t = \sigma(W_z \cdot [b_{t-1}, x_t]), \tag{10}$$

$$\tilde{b}_t = \tanh\,(W_b \cdot [r_t * b_{t-1}, x_t]), \tag{11}$$

$$b_t = (1 - z_t) * b_{t-1} + z_t * \tilde{b}_t, \tag{12}$$

$$y_t = \sigma(W_o \cdot b_t), \tag{13}$$

where r and z stand for the reset and update gates, respectively, and the current hidden layer's information and observations are used by the rearranged gate function to determine the next in-between hidden layer. The update gate determines how much the current weighted average of hidden layer data deviates from the previous value. The input-output relationship and GRU cell architecture are diagrammed in Figure 3.

Table 1: Processing factors.

Factors	Unit
Humidity	%
Temperature	˚C
Wind speed	m/s
Cloud cover	%
DNI	W/m^2

This paper makes use of the bidirectional structure. The two-way recurrent network uses both past information and predictions for the future. Neighboring neurons whose time windows extend beyond the current time step represent

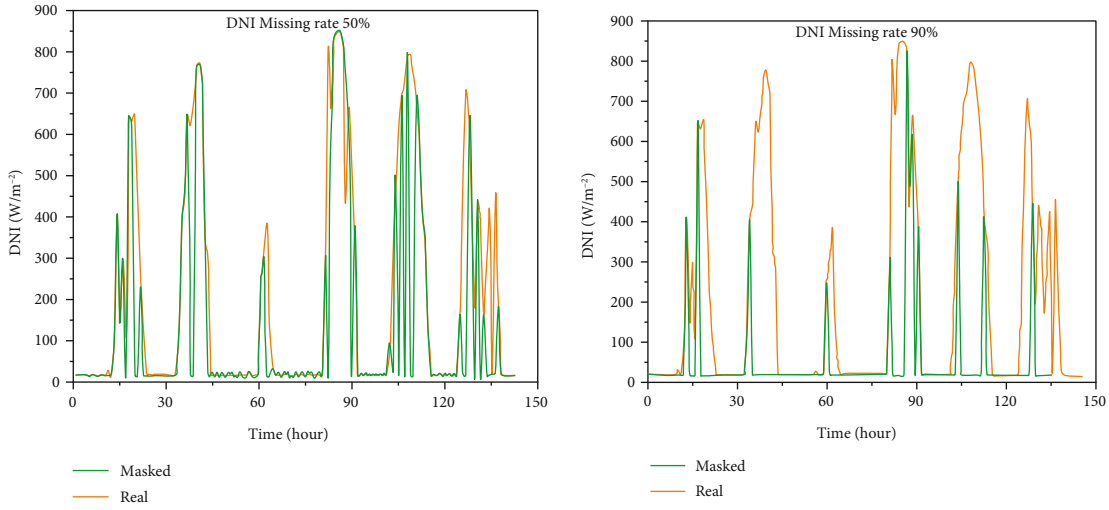

Figure 5: Incomplete data with different missing rate.

information about what will happen in the future without any data loss. Compared to regular GRU, bidirectional GRU is preferable since the factors are instantaneously defined by material from both instructions, making it worthwhile even if the assertion is primarily decided by ancient data (maximum and missing steps).

3.3.3. AIGRU. In this paper, the researcher provides the GRU model based on attention. Natural language processing (NLP) was the first area to make use of the attention mechanism [37, 38]. Its primary purpose is to quantify the degree of association between a source word and the rest of the sentence. Like in equation (9), the final hidden layer is often used as the output source. A linear combination that can be taught is allocated to the hidden layer, even if the network can remember substantial time steps from the past. In equation (14), the researcher finds the updated weights for the hidden layer [39].

$$\alpha_i = p(z = i|X, q) = \text{softmax}(s(x_i, q)) = \frac{\exp\left(s(x_i, q)\right)}{\sum_{j=1}^{N} \exp\left(s\left(x_j, q\right)\right)}. \tag{14}$$

In the interpreter, where the confidential data from the highest-order GRU layer is accessed, q is the number of queries. The weights are normalized from zero to one through the SoftMax function. The internal construction of attention and the link between its inputs and outputs are depicted in Figure 4.

3.4. Performance Evaluation Metrics. Even though RMSE is the utmost popular statistic, it is still insufficient. The following case study uses three evaluation measures, each briefly described below. The number of test samples, m, observation is denoted by y_i, whereas the prediction results are indicated by $\hat{y}_i$.

3.4.1. RMSE. The RMSE formula, equation (15), employs the square of the variation among the predicted and actual values.

$$\text{Root Mean Square Error (RMSE)} = \sqrt{\frac{1}{m}\sum_{i=1}^{m} (y_i - \hat{y}_i)^2}. \tag{15}$$

3.4.2. Mean Absolute Error (MAE). Distinct RMSE, MAE uses absolute error in equation (16). It more accurately depicts the condition of the error in the projected values than RMSE does and is not as susceptible to extreme levels. However, specific gradient optimizers find it inconvenient to utilize because the calculation cannot be distinguished.

$$\text{MAE} = \frac{1}{m}\sum_{i=1}^{m} |(y_i - \hat{y}_i)|. \tag{16}$$

3.4.3. Squared Differences between the True Value and the Mean Value. The numerator in equation (17) is the total of the squares of the discrepancies between the actual and estimated values. In this case, the summation of the squared discrepancies between the actual and the average value is represented in the denominator.

$$R^2 = 1 - \frac{\sum_i (\hat{y}_i - y_i)^2}{\sum_i (\bar{y}_i - y_i)^2}. \tag{17}$$

The reliability of a regression model may often be assessed using the R^2. The improved model estimate is associated with a higher value of R^2.

4. Results and Discussion

4.1. Data. The coordinates 39.8320 (N), 106.210 (W), and 1832.9 (meters) are the center and the edge of the target

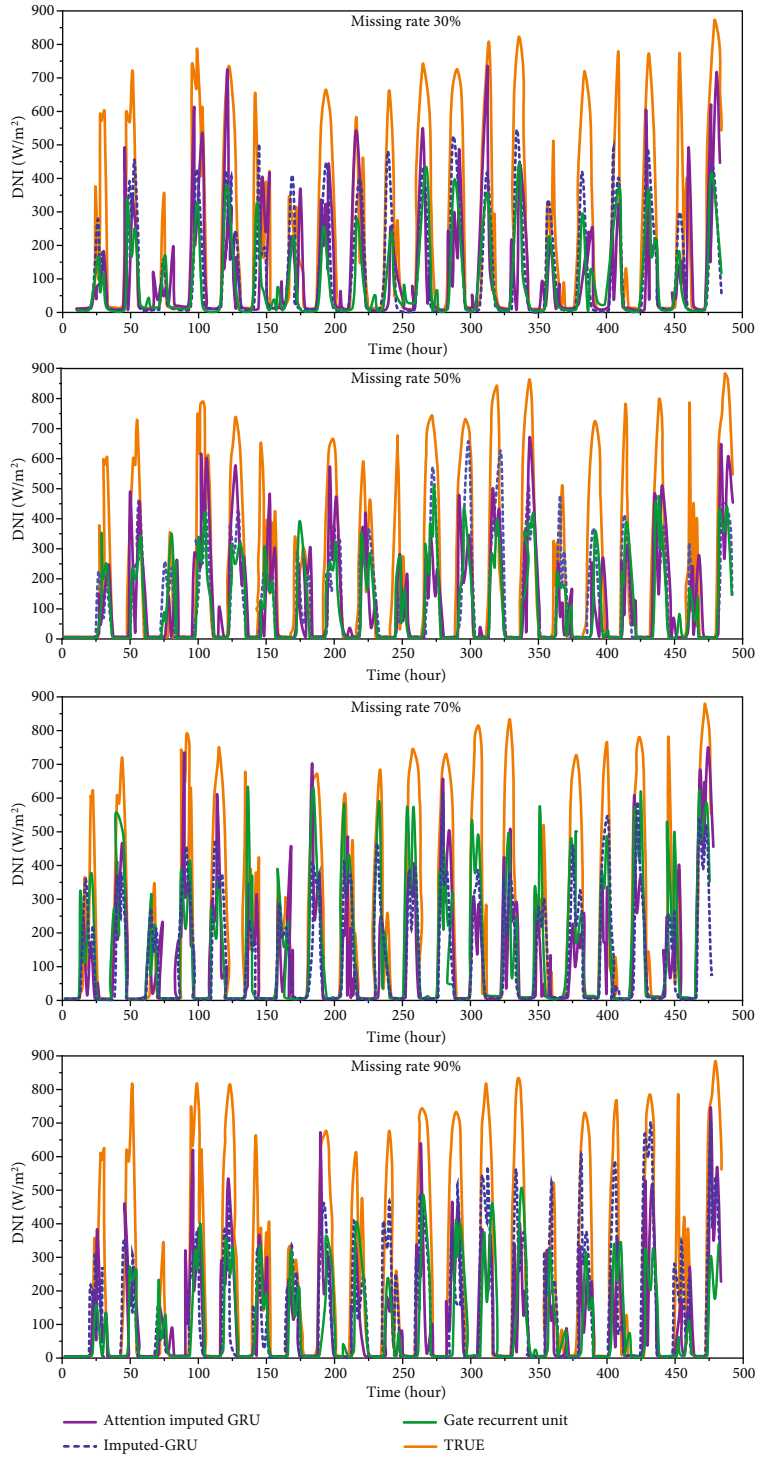

Figure 6: An outcome of AIGRU (purple), IGRU (blue), GRU (green), and observed DNI (orange).

Table 2: Error valuation.

Missing data	AIGRU	GRU	IGRU
0.30	−456.6563	−469.6538	**−407.2598**
0.50	**−391.1825**	−431.3310	−404.1761
0.70	−409.6805	−379.0675	**−329.7932**
0.90	−423.5651	−434.6867	**−348.8767**

region, respectively. The case study makes use of five sets of meteorological data, all of which are listed in Table 1.

Researchers generate the missing data at random to make the model more accurate. Here, the researcher provides a concise introduction of "missing" and its impetus. Radiometers and anemometers are just two examples of meteorological sensors used in PV facilities to measure irradiance and other weather conditions. The two most frequent

Table 3: The results of AIGRU, IGRU, and GRU.

Evaluation technique	Mean absolute error			Masked root mean squared error			Regression			Root mean square error		
	GRU	IGRU	AIGRU	GRU	IGRU	AIGRU	GRU	IGRU	AIGRU	GRU	IGRU	AIGRU
0.30	158.60	132.15	**125.72**	257.24	220.53	**209.97**	0.25	0.45	**0.49**	254.97	**223.91**	227.63
0.50	139.88	**132.28**	138.81	230.31	**220.63**	231.03	0.40	**0.44**	0.39	235.32	**228.38**	236.40
0.70	128.22	**117.81**	124.70	211.09	**199.74**	208.02	0.49	**0.54**	0.51	212.40	**201.58**	228.89
0.90	140.45	**121.46**	126.27	234.33	**200.13**	213.66	0.37	**0.54**	0.48	241.16	**208.15**	231.03

maintenance voids are single-point voids and segmented voids. The most frequent cause of a single missing point is a malfunctioning instrument, while the most frequent reason for a segmented missing is a severed line of communication. Because of the warning systems and routine checks, these outages never last more than a day. In Figure 5, the researcher saw the synthetic DNI researcher generated, with the missing data at varying percentages. When the interest rate is high, the situation is reversed. When there is a lot of missing data, it is not easy to conclude anything, such as when irradiance levels are highest.

4.2. Experimental Setting. The variables used in the experiment are briefly explained below. The researcher begins with a summary of the network's settings. A GRU encoder and two linear layers make up each bidirectional GRU's three-layer structure. At present, each GRU encoder has two hidden layers. There are 32 neurons in each of the hidden layers. The linear layer performs the dimensional translation, ensuring that all networks produce the same results. An early-stopping approach is implemented alongside a prolonged learning rate of 0.001. Once the validation set loss is not minimized after 20 iterations of training, overfitting is prevented by stopping the activity. The current epoch is 100. There is a 90% training ratio, a 16% validation rate, and a 4% testing rate.

4.3. Case Study. During this section, the researcher reclaims the case study. Starting with the past four days of radiation ranges and weather information, our studies use numerous input solitary outputs to predict the next 4 hours of diffuse near-infrared illumination (DNI). Considering the current state of affairs, the lack of irradiance is set at 50%, while the percentage of other meteorological parameters that are absent varies from 30% to 90%. In contrast to imputation tasks, predictions made without sufficient background knowledge are meaningless. There is also little chance of a significant number of missing due to maintenance with the primary variable monitors. Increasing the training sample can overcome the problem of missing data, even if there is a lot of it in a short time.

4.3.1. Evaluation among AIGRU, GRU, and IGRU. The findings are primarily analyzed using the three most typical parameters: temperature, wind speed, and DNI. The outcomes for the 30, 50, 70, and 90% missing rates are depicted in Figure 6. The test sequence is 20 days long, and the vertical axis represents the DNI power (500 W/m^2). If looking for an approach that gets the researcher closer to the actual numbers, IGRU is the best result. In Table 2, the researcher saw the average inaccuracy of the methods when the actual DNI is more significant than 500 W/m^2. Improved results are seen across a range of missing rates when using the proposed strategy.

This suggests that IGRU can improve its predictions. There is no significant difference in performance between the three approaches when the missing data rate is 30%. When the light intensity is high, AIGRU performs well. The most important goal is that the consideration module directs the model's attention to the most important objectives when there is enough accurate data. IGRU outperforms MSE in three additional scenarios with varying missing rates. The three scenarios are (1) evaluating model performance, (2) image processing, and (3) signal processing.

The inaccuracy of three approaches across four evaluation measures is shown in Table 3. Systems that include a neural imputation module improve on average by 4-18% in RMSE compared to methods that do not, with IGRU outperforming the competition. At a 30% missing rate, AIGRU is superior to IGRU in all measures except RMSE. One possible explanation is that the model can better match high-energy data, such as high-irradiance data. However, as the gap grows, the imputation module's estimates become less reliable, and the data becomes more skewed. Despite this, it shows improvement over the original data without losing quality, reassuring the accuracy of the imputed values. Moreover, IGRU improves its performance as the missing rate increases, peaking at a missing rate of 90%. Weaker performance is seen from the initial strategy as the IGRU is raised higher.

The error distribution $(Y - Y^{\wedge})$ is displayed graphically through a histogram, which the researcher uses to compare the two methods. Error distributions for the suggested approaches of AIGRU and IGRU and the baseline GRU model are shown in Figure 7. When plotted, mistakes with the correct DNI are shown along the horizontal axis, while error frequency is shown along the vertical axis in the test dataset. It is generally accepted that both AIGRU and IGRU perform better than the approach without imputation due to their high frequency at zero. The proposed methods focus on the range from 200 W/m^2 to 600 W/m^2, with a greater frequency at low error density and a lower frequency at high error density. Performance-wise, AIGRU is at its finest at 30% and vilest at 70%. In the range from 260 to zero with a 70% missed rate, AIGRU is still somewhat more frequent than GRU.

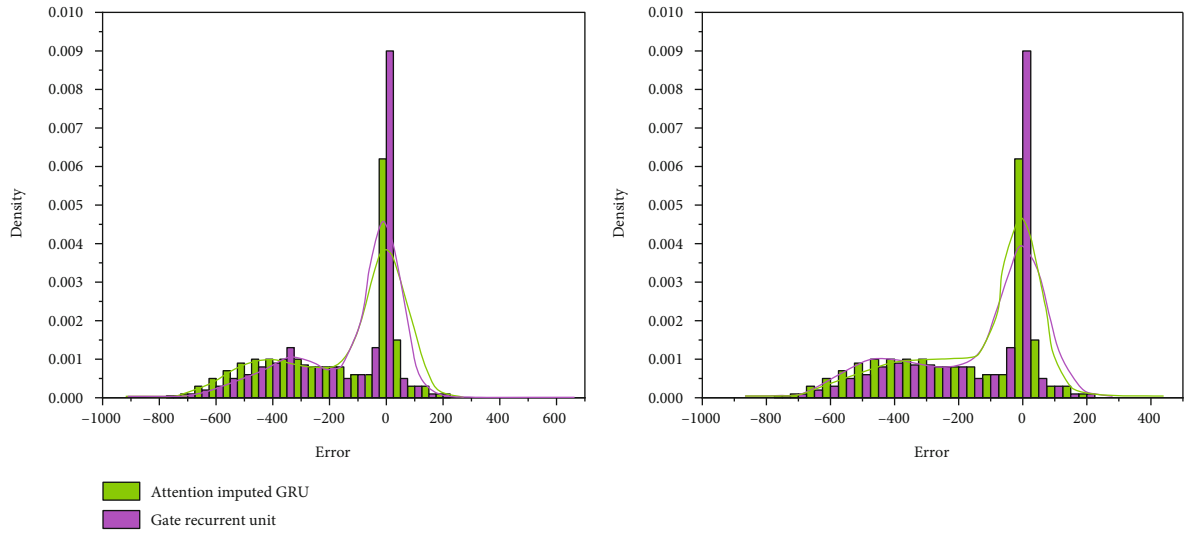

(a) 30% missing rate

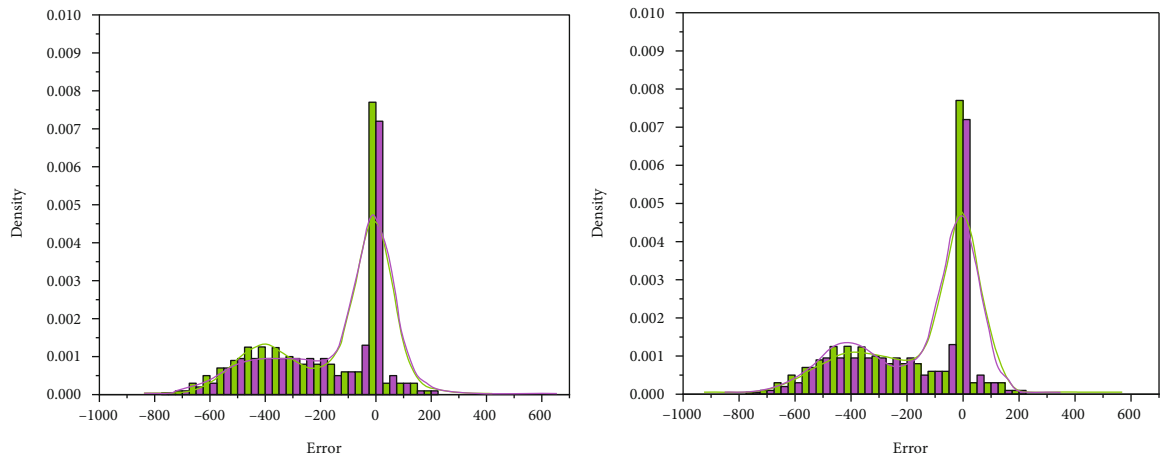

(b) 50% missing rate

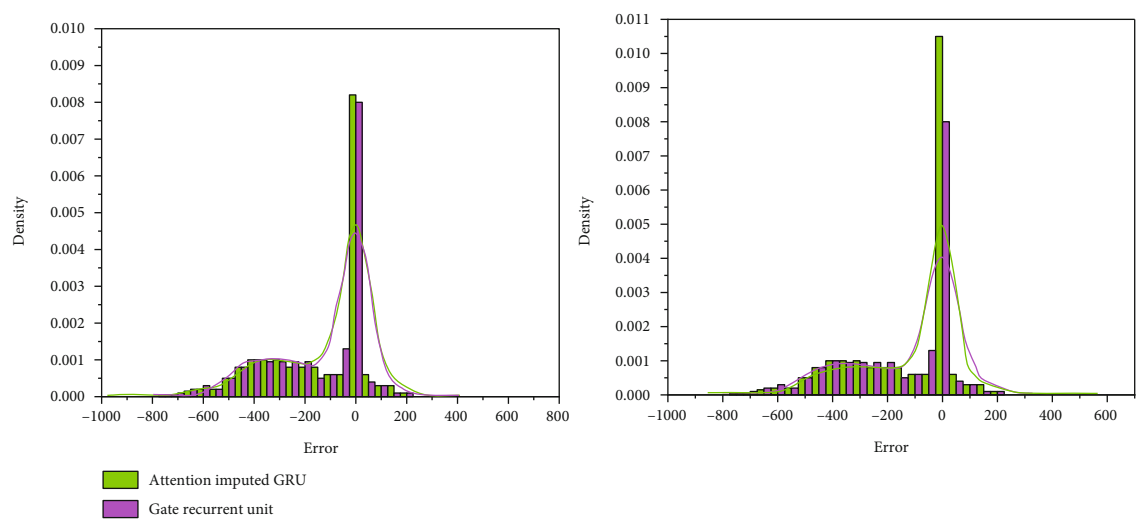

(c) 70% missing rate

Figure 7: Continued.

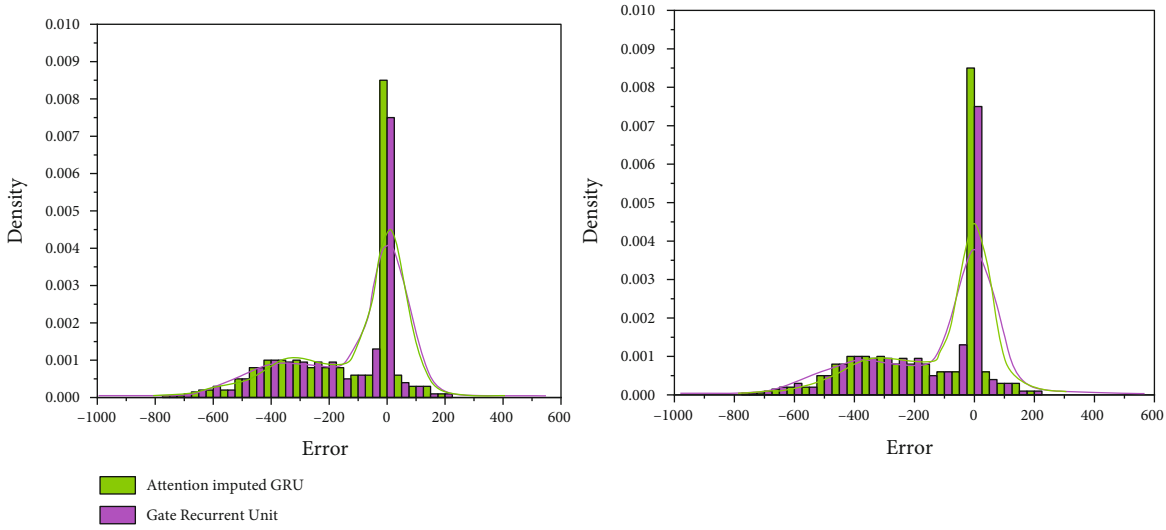

(d) 90% missing rate

Figure 7: Error histogram.

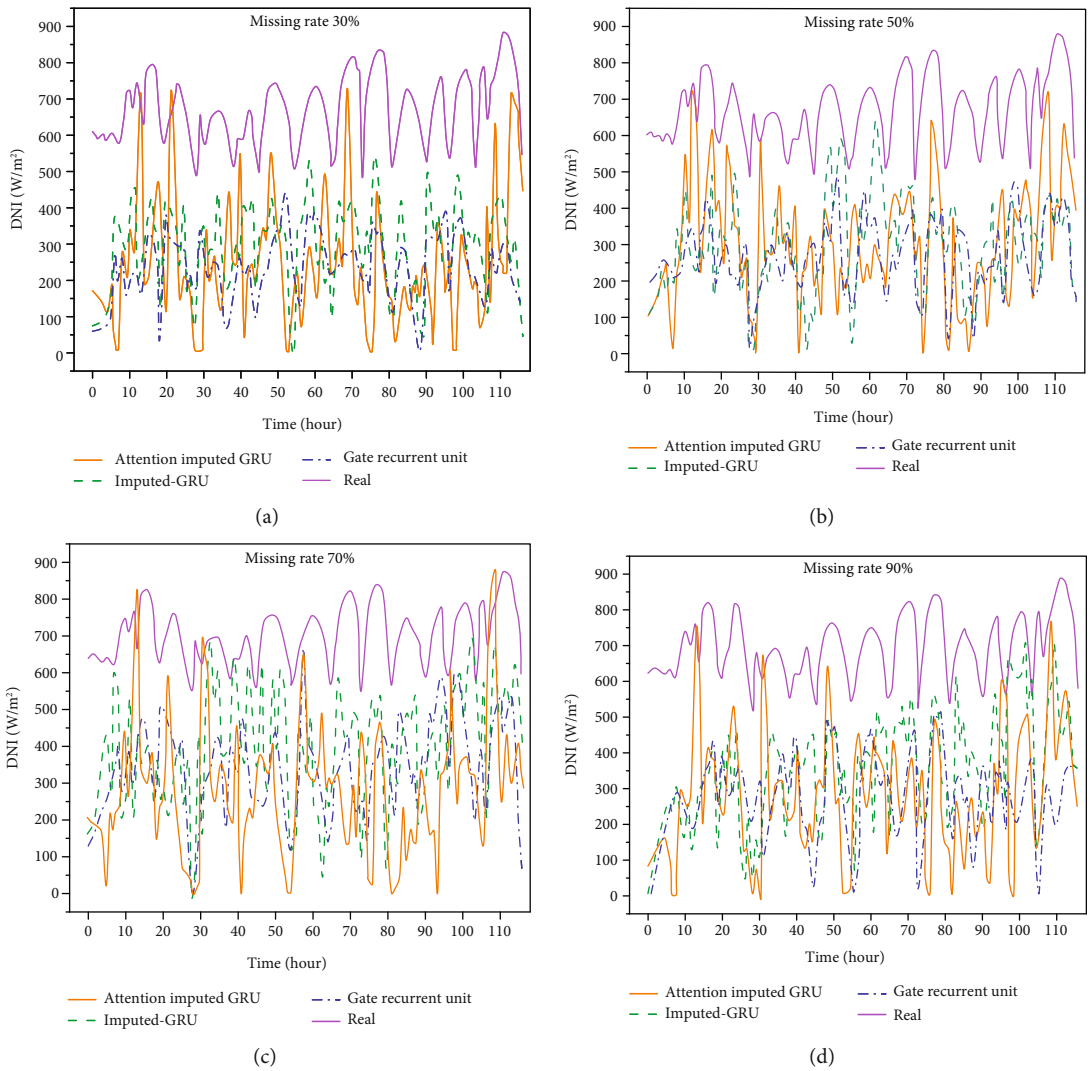

Figure 8: An outcome of AIGRU, IGRU, and GRU at higher irradiance (500 W/m^2).

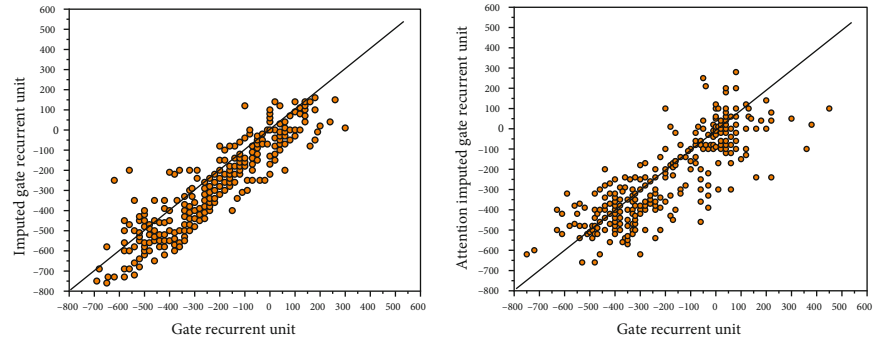

(a) 30% missing rate

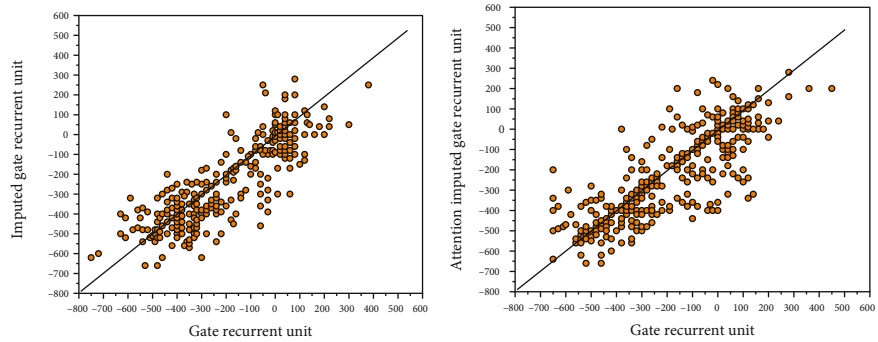

(b) 50% missing rate

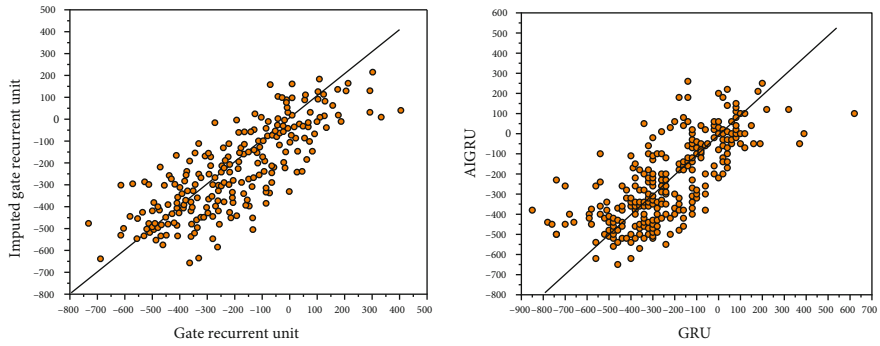

(c) 70% missing rate

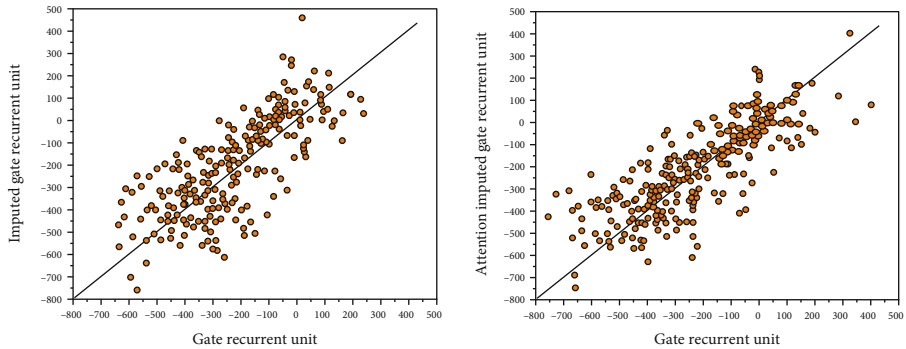

(d) 90% missing rate

Figure 9: The scatter error for various missing rates.

By either metric, AIGRU lags behind IGRU in terms of overall performance, but it pulls ahead by a wide margin when the radiation levels are high. When true DNI is more significant than 500 W/m^2, the results of the three models are shown in Figure 8. For a variety of missing rates, AIGRU is superior.

Scatter plots show the relation between the two approaches; they can be used to check this theory. In Figure 9, the GRU's blunders are shown along the horizontal axis. Possible flaws in the suggested procedures are shown in the vertical axis. Meanwhile, since $Y = X$, the mistakes

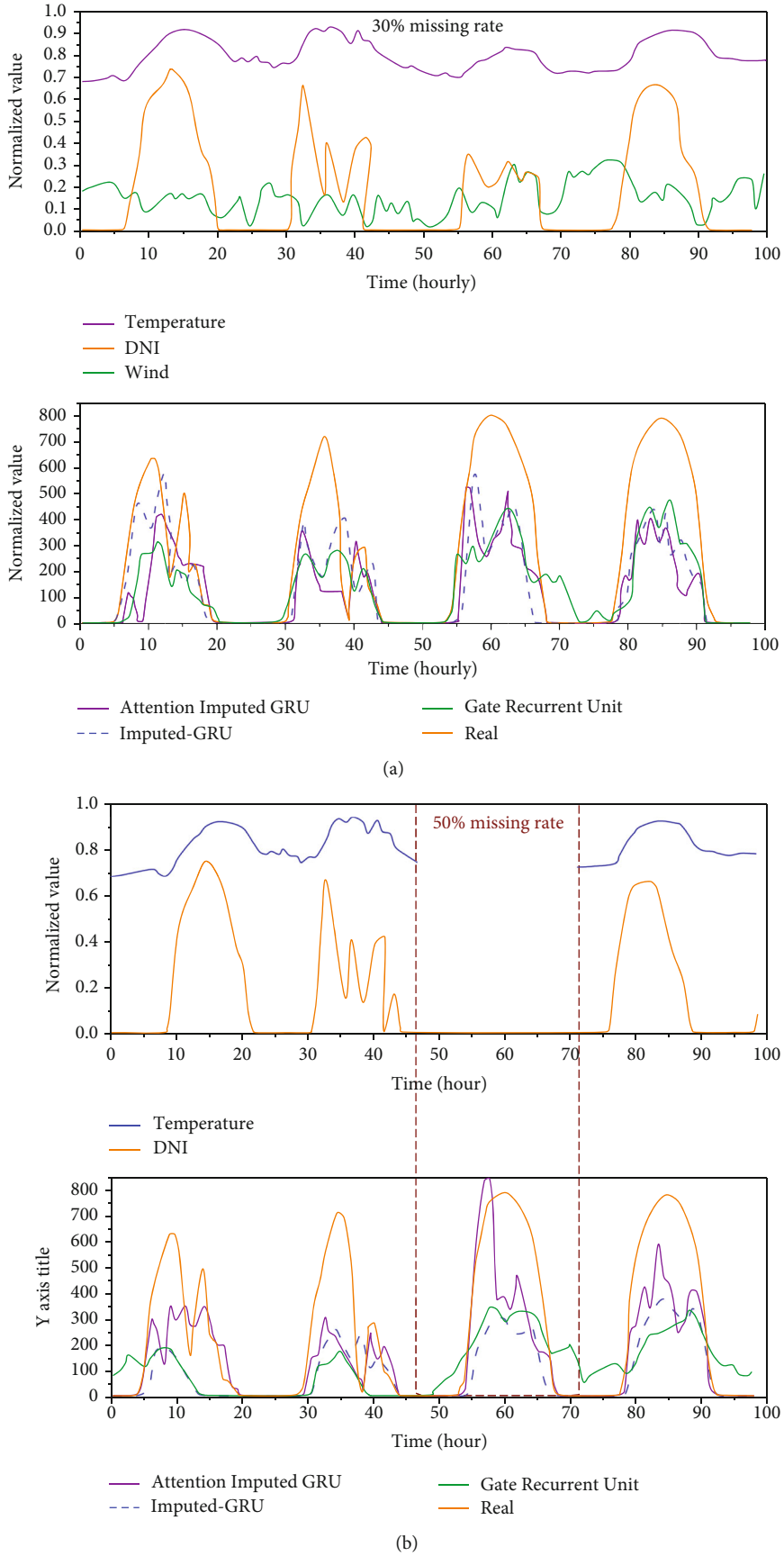

Figure 10: Continued.

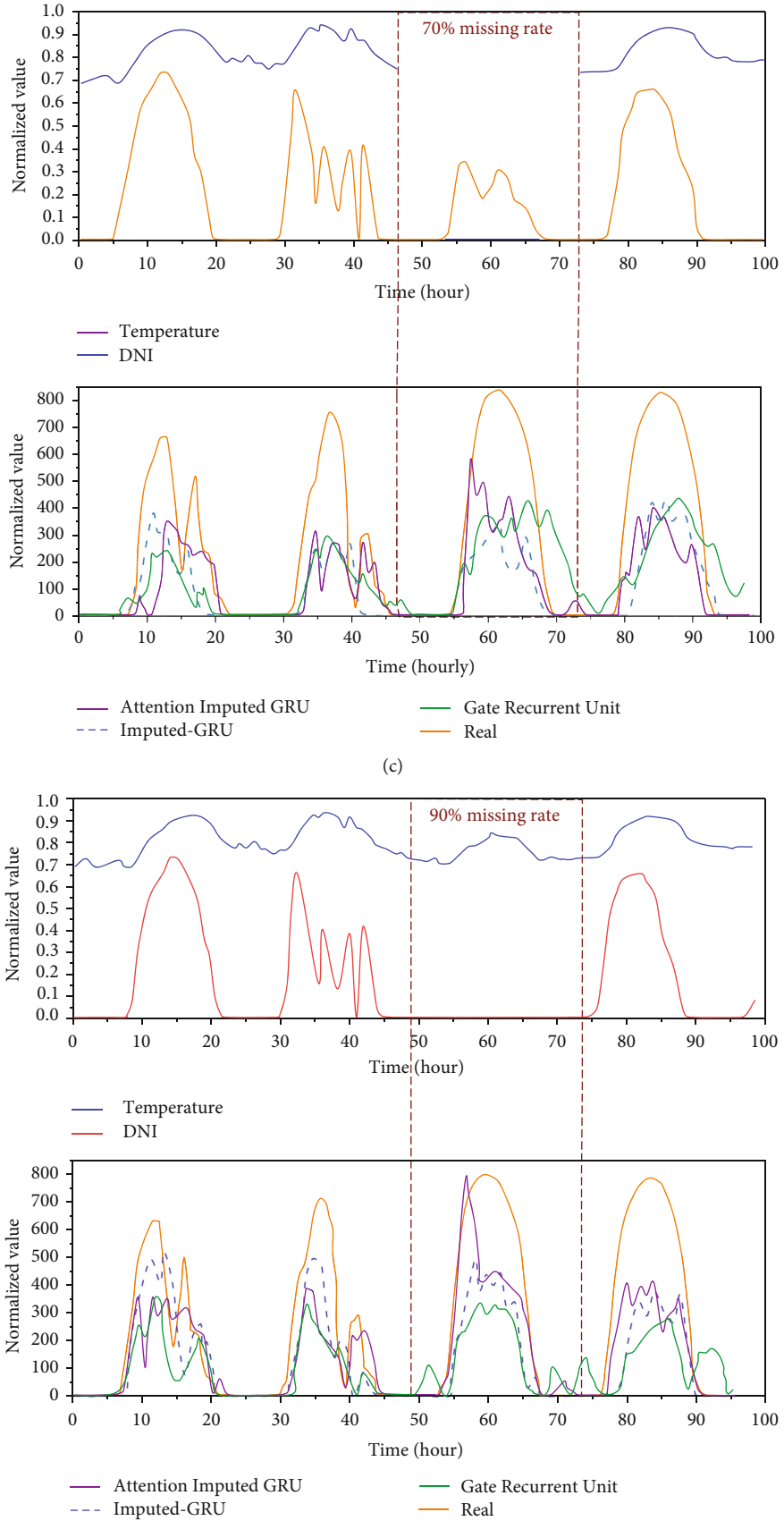

Figure 10: An outcome of variant missing design with 50% missing data.

associated with the two approaches are equivalent. The line's higher portion indicates wherever the GRU performs restored than the proposed approaches, while the line's lower part shows where the GRU serves worse. The smaller the distance between the point and the line, the more similar the two approaches are. The further the moment is from the line, the greater the method's superiority over the alternative. More data points are below the line than above, suggesting that the proposed approaches outperform GRU. When equating AIGRU and gate recurrent unit, the researcher can also see that the data under AIGRU are further spread out, which denotes that AIGRU is more precise than IGRU at forecasting specific values. For instance, in the locations near the right border, the GRU error is about 400 W/m^2, while the error in AIGRU is nearly zero. Errors of over 400 W/m^2 are possible only under extreme illumination conditions.

This finding agrees with the one drawn from the prediction mentioned in the graph. In conclusion, the attention module enables the model to pay closer attention to important details, but at the sacrifice of some average accuracy or the need for tweaks.

4.3.2. Different Missing Patterns. The impact on the model varies depending on the type of missing data. Here, the researcher undertakes tests using three frequently encountered pattern types: (1) sensor noise-related random missing (existence of short segments and sporadic missing) and (2) intervals of missing data for all variables (e.g., an entire day), most often due to technical difficulties with the network. Missing DNI segments (the primary aim), climate factor segments at random, or DNI segments with climate factor missing are all missing data in category three. In Figure 10(a), the researcher saw random missing data; somewhere, 50% of all variables are missing. Since the researcher does not see the whole picture, our model for comparing patterns is a learned one, so the researcher can only make educated guesses about what the missing design might be.

The upper figure depicts the absent Temp and DNI, while the lower figure contrasts the original GRU with the two enhanced approaches based on 96 days of data. The long history of data used and the higher model order prevent the prediction failure caused by the sporadic missing during the model inference process. Similar convincing predictions can be made by the GRU without imputation, albeit with a little lower accuracy. The third type of missing data is segmented missing data, where all input variables are blank for a given period, say, 24 hours. Figure 10(b) demonstrates the two approaches to predicting the DNI. IGRU and GRU suffer performance drops under these conditions, although AIGRU outperforms random missing. Possible explanation: accuracy suffers significantly at the expense of robustness to missing all day when utilizing more extensive historical data. Adverse effects on IGRU and AIGRU are apparent when the weather factor and typical DNI are removed. While the absence of DNI has less impact on both approaches, AIGRU obtains better results in Figures 10(c) and 10(d). Instinctively, as DNI fluctuates, it becomes clear that incorporating the weather factor into the prediction task is essential. Despite the overall decrease in loudness and smoothness of the waveform, GRU remains unaffected by these absences. As with filtering, GRU achieves a desirable smoothing outcome at the expense of precision.

Table 4: Mean absolute error valuation with three characteristics.

Missing data	MICE	Mean	MF	KF	KNN	This study
0.50	161.28	154.26	172.82	138.86	144.17	**131.43**
0.70	156.13	169.34	176.68	129.53	124.12	**118.22**
0.90	164.44	174.12	155.26	126.01	128.42	**121.81**

Table 5: Mean absolute error valuation with five characteristics.

Missing data	MICE	Mean	MF	KF	KNN	This study
0.50	162.63	162.36	187.22	**121.96**	130.31	137.81
0.70	154.57	162.58	157.23	**124.59**	131.24	151.12
0.90	179.78	188.41	140.38	133.63	145.54	**126.24**

4.3.3. Comparison with Other Imputation Techniques. To authenticate that the approaches were as reliable as advertised, the researcher expanded their range from three to five variables and tested each using a variety of interpolation schemes. Using these techniques, the researcher attributes the missing variables and sets GRU to work on the prediction. Mean interpolation, matrix complementarity, minimum irradiance consistent emulation, and K-nearest neighbor are some additional irradiance imputation methods compared in Tables 4 and 5. Two climatic elements, cloud cover and humidity, are added to the three input factors of the other group. To create this approach, the researcher combined the most valuable aspects of both IGRU and AIGRU. Here, MAE is the error of choice.

According to Table 4, the suggested technique is more accurate than the poorest imputation methods by as much as 32% and provides a 4-8% enhancement over the best imputation method. The proposed methods outperform most of the existing techniques in the case study with five contributions. When comparing KF to the suggested approach, KF performs better in the 50% and 70% missing proportion cases. On the other hand, the recommended strategy is the best option when 90% of the data is absent. In conjunction with the trivariate case, it demonstrates that KF and the suggested technique perform well under conditions with an adequate amount of reliable information. However, the proposed method exhibits higher performance with high missing rates, indicating that it is more robust. It also shows that the proposed strategy may be applied to any situation without modifying the model. However, the various data sets will still require different imputation procedures.

As the percentage of missing values rises, the performance of mean interpolation declines compared to the other approaches. In contrast, MICE and MF outcomes are data-driven.

5. Conclusion

With the help of a neural imputation module, this research suggests a new approach to predicting irradiance. In many cases, its performance is superior to the standard method and other well-known imputation techniques. The IGRU benefits from being highly adaptable, requiring no additional imputation step during data pre-processing, and having minimal computational complexity. Additionally, it is an effort to combine the imputation and prediction steps, hoping that incorporating prediction data can improve imputation. Of course, there is still much room for improvement in the field of time series imputation for renewable energy.

Irradiance readings fluctuate wildly and are significantly influenced by weather patterns. This finding demonstrates that the outcomes of various approaches vary among datasets. Traditional methods are effective when the targets are easy to hit. It is still worthwhile to study imputation techniques, especially under challenging conditions like heavy rain or other extreme weather. Because of this, the imputation module can benefit from encoding feature correlations by investigating more explicit model properties, such as fundamental relationships among components and time graph relations among its parts.

For optimal performance in the field, the imputation architecture should be fine-tuned using real-world applications, such as irradiance prediction and missing data states for power prediction in photovoltaic plants. Designing temporal windows with flexibility, interpolating data in real-time, using multiple modalities, and other strategies are all viable alternatives. The model parameters can also be adjusted to make it more generalizable.

Data Availability

All data supporting the findings of this study are included in this article.

Ethical Approval

All procedures performed in this study involving human participants were in accordance with the ethical standards of the institutional and/or national research committee and its later amendments or comparable ethical standards.

Disclosure

The funders had no role in the study design, data collection, and analysis, decision to publish, or manuscript preparation.

Conflicts of Interest

The authors declare that they have no competing financial interest conflicts in this paper.

References

[1] G. Narvaez, L. F. Giraldo, M. Bressan, and A. Pantoja, "Machine learning for site-adaptation and solar radiation forecasting," *Renewable Energy*, vol. 167, pp. 333–342, 2021.

[2] L. S. Hoyos-Gómez, J. F. Ruiz-Muñoz, and B. J. Ruiz-Mendoza, "Short-term forecasting of global solar irradiance in tropical environments with incomplete data," *Applied Energy*, vol. 307, article 118192, 2022.

[3] Q.-T. Phan, Y.-K. Wu, Q.-D. Phan, and H.-Y. Lo, "A study on missing data imputation methods for improving hourly solar dataset," in *2022 8th International Conference on Applied System Innovation (ICASI)*, pp. 21–24, Nantou, Taiwan, 2022.

[4] E. Miranda, J. F. G. Fierro, G. Narváez, L. F. Giraldo, and M. Bressan, "Prediction of site-specific solar diffuse horizontal irradiance from two input variables in Colombia," *Heliyon*, vol. 7, no. 12, article e08602, 2021.

[5] L. Wang and J. Shi, "A comprehensive application of machine learning techniques for short-term solar radiation prediction," *Applied Sciences*, vol. 11, no. 13, 2021.

[6] A. Kocian, G. Carmassi, F. Cela, L. Incrocci, P. Milazzo, and S. Chessa, "Bayesian sigmoid-type time series forecasting with missing data for greenhouse crops," *Sensors*, vol. 20, no. 11, 2020.

[7] D. P. Choudhary, A. C. Cadavid, A. Cookson, and G. A. Chapman, "Variability in irradiance and photometric indices during the last two solar cycles," *Solar Physics*, vol. 295, no. 2, 2020.

[8] M. Alqudah, T. Dokic, M. Kezunovic, and Z. Obradovic, "Prediction of solar radiation based on spatial and temporal embeddings for solar generation forecast," 2022, http://arxiv.org/abs/2206.08832.

[9] C. Rizos-Theodoros and A. F. Bais, "Determination of Uncertainty in Hourly and Daily Averages of Solar Irradiance Due to Missing Measurements," *AIP Conference Proceedings*, vol. 2075, 2019.

[10] M. David, M. A. Luis, and P. Lauret, "Comparison of intraday probabilistic forecasting of solar irradiance using only endogenous data," *International Journal of Forecasting*, vol. 34, no. 3, pp. 529–547, 2018.

[11] H. Alam, M. Y. Mashor, M. Irwanto et al., "Output characteristics of photovoltaic module in Medan based on estimated solar irradiance using hargreaves method for application assessment of transformerless photovoltaic inverter," in *AIP Conference Proceedings*, AIP Publishing, 2016.

[12] T. D. De Wit, "A method for filling gaps in solar irradiance and solar proxy data," *Astronomy & Astrophysics*, vol. 533, p. A29, 2011.

[13] M. Kumar, K. Namrata, and N. Kumari, "Hyper-parametric improved machine learning models for solar radiation forecasting," *Concurrency and Computation: Practice and Experience*, vol. 34, no. 23, 2022.

[14] S. A. Haider, M. Sajid, H. Sajid, E. Uddin, and Y. Ayaz, "Deep learning and statistical methods for short- and long-term solar irradiance forecasting for Islamabad," *Renewable Energy*, vol. 198, pp. 51–60, 2022.

[15] X. Jiao, X. Li, D. Lin, and W. Xiao, "A graph neural network based deep learning predictor for spatio-temporal group solar irradiance forecasting," *IEEE Transactions on Industrial Informatics*, vol. 18, no. 9, pp. 6142–6149, 2022.

[16] Y. Su, N. Li, H. Yang et al., "A feature importance analysis based solar irradiance mapping model using multi-channel satellite remote sensing data," in *2022 IEEE/IAS 58th Industrial and Commercial Power Systems Technical Conference (I&CPS)*, Las Vegas, NV, USA, 2022.

[17] O. Bamisile, A. Oluwasanmi, C. Ejiyi, N. Yimen, S. Obiora, and Q. Huang, "Comparison of machine learning and deep

learning algorithms for hourly global/diffuse solar radiation predictions," *International Journal of Energy Research*, vol. 46, no. 8, pp. 10052–10073, 2022.

[18] B. Brahma and R. Wadhvani, "Visualizing solar irradiance data in ArcGIS and forecasting based on a novel deep neural network mechanism," *Multimedia Tools and Applications*, vol. 81, no. 7, pp. 9015–9043, 2022.

[19] A. Abubakar Mas'ud, "Comparison of three machine learning models for the prediction of hourly PV output power in Saudi Arabia," *Ain Shams Engineering Journal*, vol. 13, no. 4, 2022.

[20] W. Bendali, I. Saber, B. Bourachdi, M. Boussetta, and Y. Mourad, "Deep learning using genetic algorithm optimization for short term solar irradiance forecasting," in *2020 Fourth International Conference On Intelligent Computing in Data Sciences (ICDS)*, Fez, Morocco, 2020.

[21] T.-P. Chu, J.-H. Jhou, and Y.-G. Leu, "Image-based solar irradiance forecasting using recurrent neural networks," in *2020 International Conference on System Science and Engineering (ICSSE)*, Kagawa, Japan, 2020.

[22] S. Shan, X. Xie, T. Fan et al., "A deep-learning based solar irradiance forecast using missing data," *IET Renewable Power Generation*, vol. 16, no. 7, pp. 1462–1473, 2022.

[23] S. Syama and J. Ramprabhakar, "Multistep ahead solar irradiance and wind speed forecasting using Bayesian optimized long short term memory," in *2022 7th International Conference on Communication and Electronics Systems (ICCES)*, Coimbatore, India, 2020.

[24] G. L. Martins, R. A. Campos, M. Braga, and R. Rüther, "Implementing k-Nearest Neighborhood as a forecast method for Intra hour resolution with no exogenous outputs," in *Proceedings of the ISES Solar World Congress 2019*, pp. 2109–2114, Germany, 2020.

[25] H. Farahneh, F. Hussian, and X. Fernando, "De-noising scheme for VLC-based V2V Systems; a machine learning approach," *Procedia Computer Science*, vol. 171, pp. 2167–2176, 2020.

[26] S. Saha, N. Majumder, D. Sangani, and A. Das Bhattacharjee, "Comprehensive forecasting-based analysis using hybrid and stacked stateful/stateless models," *Lecture Notes in Networks and Systems*, vol. 427, pp. 567–579, 2022.

[27] N. P. Sebi, "Intelligent Solar Irradiance Forecasting Using Hybrid Deep Learning Model: A Meta-Heuristic-Based Prediction," *Neural Processing Letters*, vol. 55, no. 2, pp. 1247–1280, 2023.

[28] B. Zhou, S. Du, L. Li, H. Wang, Y. He, and D. Zhou, "An explainable recurrent neural network for solar irradiance forecasting," in *2021 IEEE 16th Conference on Industrial Electronics and Applications (ICIEA)*, pp. 1299–1304, Chengdu, China, 2021.

[29] F. R. Alharbi and D. Csala, "Short-term solar irradiance forecasting model \based on bidirectional long short-term memory deep learning," in *2021 International Conference on Electrical, Communication, and Computer Engineering (ICECCE)*, Kuala Lumpur, Malaysia, 2021.

[30] X. Huang, Q. Li, Y. Tai et al., "Hybrid deep neural model for hourly solar irradiance forecasting," *Renewable Energy*, vol. 171, pp. 1041–1060, 2021.

[31] S. Sharda, M. Singh, and K. Sharma, "RSAM: robust self-attention based multi-horizon model for solar irradiance forecasting," *IEEE Trans Sustain Energy*, vol. 12, no. 2, pp. 1394–1405, 2021.

[32] M. Abdel-Nasser, K. Mahmoud, and M. Lehtonen, "Hifa: promising heterogeneous solar irradiance forecasting approach based on kernel mapping," *IEEE Access*, vol. 9, pp. 144906–144915, 2021.

[33] C. N. Obiora, A. Ali, and A. N. Hasan, "Forecasting hourly solar irradiance using long \short-term memory (LSTM) network," in *2020 11th International Renewable Energy Congress (IREC)*, Hammamet, Tunisia, 2020.

[34] D. Knol, F. de Leeuw, J. F. Meirink, and V. V. Krzhizhanovskaya, "Deep learning for solar irradiance nowcasting: a comparison of a recurrent neural network and two traditional methods," in *Lecture Notes in Computer Science (including subseries Lecture Notes in Artificial Intelligence and Lecture Notes in Bioinformatics), vol. 12746 LNCS*, pp. 309–322, Springer International Publishing, Cham, 2021.

[35] D. Kumar, H. D. Mathur, S. Bhanot, and R. C. Bansal, "Forecasting of solar and wind power using LSTM RNN for load frequency control in isolated microgrid," *International Journal of Modelling and Simulation*, vol. 41, no. 4, pp. 311–323, 2021.

[36] R. A. Rajagukguk, R. A. A. Ramadhan, and H.-J. Lee, "A review on deep learning models for forecasting time series data of solar irradiance and photovoltaic power," *Energies*, vol. 13, no. 24, 2020.

[37] Q. Ashfaq, A. Ulasyar, H. S. Zad, A. Khattak, and K. Imran, "Hour-ahead global horizontal irradiance forecasting using long short term memory network," in *2020 IEEE 23rd International Multitopic Conference (INMIC)*, Bahawalpur, Pakistan, 2020.

[38] B. Brahma and R. Wadhvani, "Solar irradiance forecasting based on deep learning methodologies and multi-site data," *Symmetry*, vol. 12, no. 11, p. 1830, 2020.

[39] H. He, N. Lu, Y. Jie, B. Chen, and R. Jiao, "Probabilistic solar irradiance forecasting via a deep learning-based hybrid approach," *IEEJ Transactions on Electrical and Electronic Engineering*, vol. 15, no. 11, pp. 1604–1612, 2020.